In-situ hierarchical pore engineering in small pore zeolite via methanol-mediated NH_4F etching

Youdong Xing, Guangchao Li*, Zezhou Lin, Zhihang Xu, Haitao Huang, Ye Zhu, Shik Chi Edman Tsang, Molly Meng-Jung Li*

Youdong Xing, Guangchao Li, Zezhou Lin, Zhihang Xu, Haitao Huang, Ye Zhu, Molly Meng-Jung Li
Department of Applied Physics, The Hong Kong Polytechnic University, Hung Hom, Hong Kong (P. R. China)
E-mail: molly.li@polyu.edu.hk, guangchao.li@polyu.edu.hk

Shik Chi Edman Tsang
Wolfson Catalysis Centre, Department of Chemistry, University of Oxford, Oxford OX1 3QR, U.K.

Hydrolysis-Activated In-situ Pore Engineering in Zeolites: NH_4F in Methanol as a Deceptively Inert Agent for a Trojan Horse-like Introduction and Activation

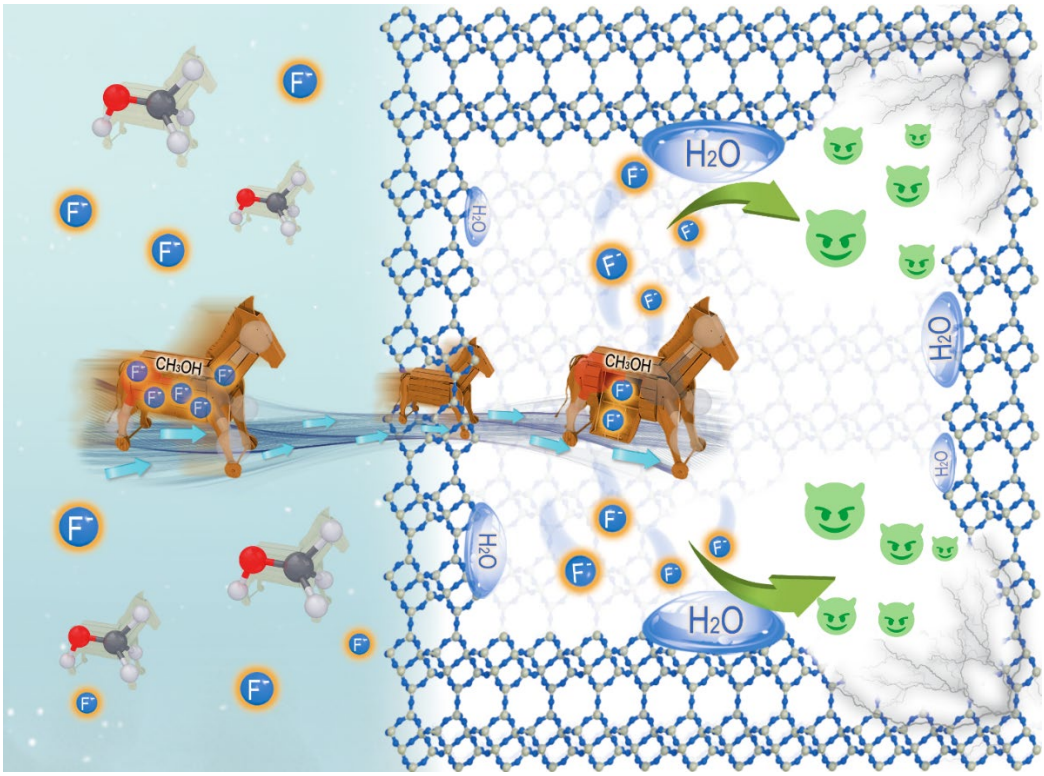

Abstract

Hierarchical zeolites have attracted significant attention from both academic and industrial communities due to their exceptional mass transport and accessibility to active sites while maintaining the shape selectivity of the zeolite. However, creating a hierarchical structure over small-pore zeolites remains a formidable challenge. In this study, we propose a novel approach that utilizes the methanol-mediated NH_4F etching method to fabricate hierarchical SSZ-13 zeolite with well-distributed mesopores. Unlike the conventional aqueous NH_4F etching process, the utilization of methanol as a solvent allows for the effective suppression of NH_4F reactivity during its transport into the zeolite channels. NH_4F remains inactive until exposed to resident water molecules in zeolite, and the subsequent hydrolysis process in situ activates the release of etching species, effectively eliminating the framework Si and Al species and allowing for uniform and controllable etching. Solid-state nuclear magnetic resonance spectroscopy provides in-depth insight into the etchant interactions with the framework defect sites and the evolution of aluminate and silicate species from framework to extra-framework, elucidating the structural and chemical changes occurring during the process. Our work presents an efficient strategy for the preparation of hierarchical zeolites with well-dispersed mesopores, offering opportunities for tailored pore engineering and holding potential for various applications such as catalysis, adsorption, and separation.

Introduction

Zeolites, which normally contain molecule-sized channels and cages of less than 2 nm, are widely used as solid heterogeneous catalysts due to their unique pore structure and high surface area.[1] These nano/sub-nano channels provide a confined environment around the active sites, such as Brønsted acid sites, which regulate the activity and selectivity of the zeolites by influencing the stability of the reactive transition states and imparting shape selectivity on reactants or products.[2-4] However, the exclusive presence of micropores often causes limited mass transport and restricted access to acid/active sites for the reactant and product molecules,[5] which are major drawbacks in most industrial reactions catalyzed by zeolites, including cracking, oxidation, alkylation, esterification, and isomerization.[6] These limitations significantly restrict the achievable catalytic performance of zeolites.[7]

To improve the effectiveness of zeolites in industrial reactions, hierarchical zeolites with tailored mesoporosities integrated with intrinsic microporosities have been synthesized using various strategies over the past few decades.[8-9] These strategies can be broadly categorized into post-treatment and template synthesis routes. Post-treatment methods, including steaming,[10-11] and acid or alkaline leaching,[12-13] are often considered more environmentally friendly than template synthesis strategy, as they do not require expensive organic templates and are more readily scalable.[14] These characteristics make post-treatment methods an attractive option for synthesizing hierarchical zeolites.

The NH_4F-based zeolite post-treatment etching process, recently developed by the Valtchev group,[15] has become popular in the engineering of hierarchical zeolites. When NH_4F is added to an aqueous solution, it forms bifluoride ions (HF_2^-) through double hydrolysis.[16] These ions can then unselectively eliminate both framework Si and Al atoms, making this process applicable to many types of zeolites, including FAU,[17-18] Mordenite,[19] CHA,[20] MFI,[21] FER,[22] and LTA,[23] etc. For example, after treating with NH_4F aqueous solution, Y zeolite exhibits improved hydroconversion of n-octane due to opened sodalite cages and increased accessibility to the acid sites.[18] It has also been demonstrated that the consecutive oxalic acid and NH_4F treatment enable hierarchical pore

structure in MOR zeolite, which enhances the catalytic performance due to substantially improved intra-particle diffusion.[19]

However, it is noteworthy that the etching processes using NH_4F aqueous solution are significantly controlled by the diffusion of active etching species, which are formed in the solution after the hydrolysis of NH_4F. Besides, the already existing active species in NH_4F aqueous solutions tend to cluster together through hydrogen bonding with H_2O and NH_4^+, which further increases the diffusion resistance and limits the accessibility into the zeolite's interior.[23] This difficult diffusion leads to the characteristic behaviours where etching typically initiates at the outer surface and subsequently progresses into the interior of the zeolite crystal. As a result, a significant concentration gradient of etching species forms within the zeolite. This, in turn, results in a highly irregular pore structure and a less ordered mesoporous system with pore size distributions ranging from 10nm to 100nm.[15, 23-24]

The diffusion resistance is especially significant in small-pore zeolites such as LTA and CHA zeolites, which have narrow intrinsic 8-membered ring windows (0.38 nm).[23, 25] In literature, various etching parameters have been carefully attempted, such as temperature, liquid-solid ratio, concentration, and etching time,[26] however, the etching process in small-pore SSZ-13 zeolites remains primarily on the outside surface and does not affect the internal frameworks. Similar results have also been observed in LTA and TON zeolites.[23] Therefore, creating hierarchical structures for small-pore zeolites using post-treatment methods while protecting the surface porous framework is still a major challenge, and there is a high demand for solutions that can result in uniform and controllable pore engineering.

In this study, we introduce a novel hydrolysis-triggered in-situ pore engineering strategy in small pore zeolites. Our approach involves utilizing methanol as a solvent to transport NH_4F into the zeolite channel. This unique solvent choice, with its higher wettability for zeolites compared to water, facilitates efficient diffusion. Importantly, the solvated F^- ions in methanol remain inert and do not react destructively with the framework wall of silicon-based materials,[27-29] thereby preventing heterogeneous etching caused by diffusion resistance. Upon contact with resident water molecules within the zeolite micropores, NH_4F undergoes in-situ hydrolysis, resulting in the release of active etching species that eliminate the framework Si and Al atoms. We refer to this approach as the Trojan Horse-like Introduction and Activation Strategy. Small-pore SSZ-13 zeolite is selected as a demonstrative example to showcase the effectiveness of the methanol-mediated NH_4F post-treatment. Our in-situ pore engineering strategy achieves a homogeneous etching process throughout the outer and inner surfaces of the zeolite. The results reveal a well-defined mesoporous structure with a narrow pore size distribution (approximately 7 nm) while preserving the zeolite's intrinsic micropore feature and morphology integrity. We also use solid-state resonance nuclear magnetic spectroscopy (SSNMR) to unravel the atomic-level etching mechanism and pore formation process. The results demonstrate that the process of pore engineering is initiated at the sites of framework-associated Al-OH and silanols (common defects sites in zeolite), resulting in initial fluoridation species, i.e., Al-F and Si-F. These fluoridated species act as intermediates that undergo subsequent transformations into octahedral extra-framework Si or Al species as the etching process progresses, leading to the formation of mesopores. Our strategy offers a significant improvement over previous fluoride post-treatment approaches and provides a promising solution for uniform and controllable hierarchical pore engineering in zeolites.

Results and discussion

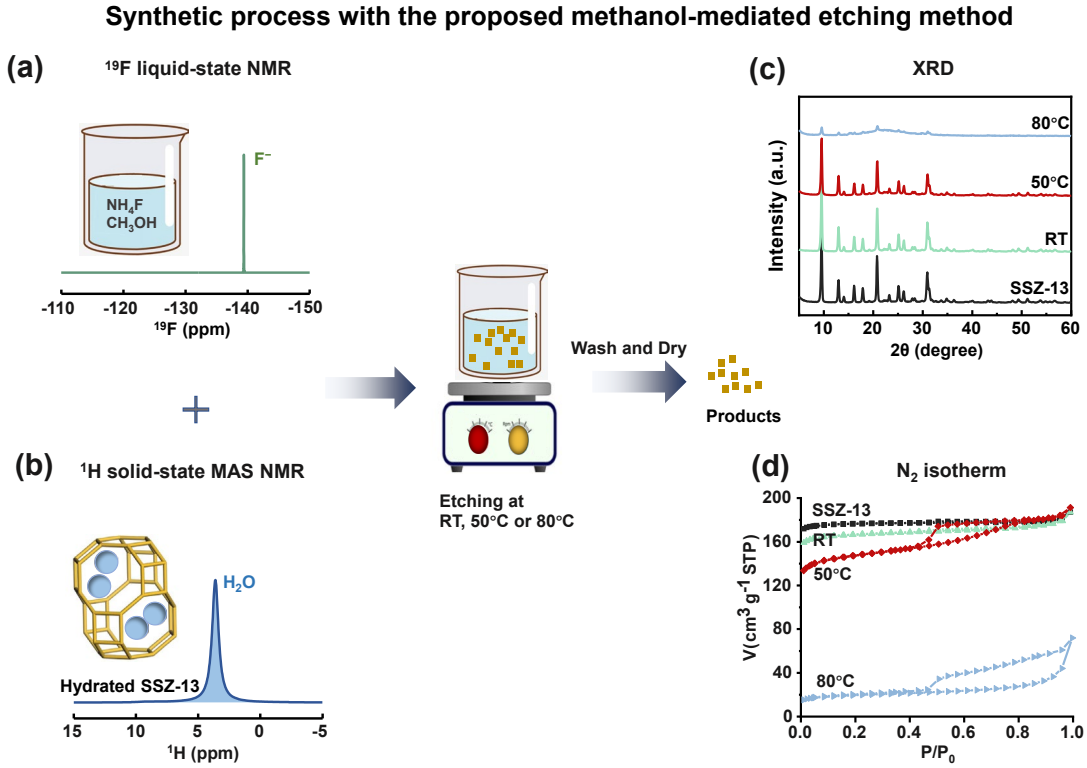

Figure 1. Illustration of the synthetic process with the proposed etching method. (a) ^{19}F liquid-state NMR spectrum of NH_4F (3.5 wt%) dissolved in methanol. (b) ^{1}H MAS SSNMR spectrum of the hydrated SSZ-13. (c) XRD patterns and (d) N_2 adsorption/desorption isotherms of SSZ-13 and NH_4F-treated samples at room temperature (RT), 50°C and 80°C.

The synthetic procedure and conditions for conducting methanol-mediated NH_4F post-treatment are shown in **Figure 1**. The ^{19}F liquid-state NMR spectrum (**Figure 1a**) confirms that the NH_4F methanol solution (NH_4F 3.5 wt%) exists in the form of F^- anions, as evidenced by a single peak at -139 ppm.[30-31] This observation indicates the effective dissolution of NH_4F in methanol. Additionally, the choice of methanol as a solvent, with its higher wettability for zeolites compared to water (as confirmed by the contact angle experiment, **Figure S1**), facilitates efficient diffusion. It is worth noting that other solvents such as ethanol can also dissolve NH_4F and potentially offer similar functionality (**Figure S2**).[31] Unlike bifluoride ions, F^- anions are not nucleophilic species[27-29] and cannot cause destruction to the zeolite framework atoms. To facilitate in situ hydrolysis of F^-/NH_4F in SSZ-13 channels and enable etchant release, hydrated SSZ-13 zeolite, as confirmed by the ^{1}H MAS SSNMR spectrum (**Figure 1b and Figure S3**), is used. Unless otherwise specified, all the SSZ-13 mentioned in the following refer to the hydrated SSZ-13. After mixing the SSZ-13 with the NH_4F methanol solution at room temperature (RT), the resulting mixture demonstrates a homogeneous distribution of fluorine in SSZ-13, as confirmed by TEM-EDS mapping (**Figure S4**).[18] Subsequently, the suspension is exposed to various temperatures (RT, 50°C, and 80°C). The NH_4F-etched samples then undergo washing and drying before analysis using XRD and N_2 adsorption/desorption isotherms. XRD patterns of the samples treated at RT and 50°C closely resemble the pristine SSZ-13 (**Figure 1c**), indicating the preservation of the crystal structure at these temperatures. However, treatment at 80°C causes the characteristic peaks of SSZ-13 to nearly vanish, suggesting structural collapse resulting from intense etching at higher temperatures. N_2

adsorption/desorption isotherms (**Figure 1d)** show that the mesopore structure only appears after treatment at 50°C and 80°C. The sample treated at RT exhibits a micropore structure similar to the pristine SSZ-13, implying that the etching process requires elevated temperatures to become effective. However, the 80°C treated sample shows the disappearance of micropore features (low N_2 uptake in the low-pressure region of $P/P_0 < 0.1$), presumably due to severe damage and framework collapse in SSZ-13, consistent with the XRD findings. From the above results, the 50°C treated sample is the only one displaying a combination of types I and IV isotherms with a distinct hysteresis loop (**Figure 1d**), indicating the formation of a bimodal (hierarchical) pore structure with both micropores and mesopores while maintaining good crystallinity. Therefore, we select 50°C as the etching temperature and prepare a series of samples with NH_4F concentrations of 0.5 wt%, 1.7 wt%, and 3.5wt%, denoted as MF-0.5, MF-1.7, and MF-3.5, respectively, to investigate the influence of NH_4F content on the resulting pore structure. For comparison, a sample treated with conventional NH_4F aqueous solution is synthesized under 50°C and denoted as WF-3.5. Notably, the alkalinity in the NH_4F methanol solution as a significant contributor to mesopore formation is excluded (**Figure S5 and Table S1**).

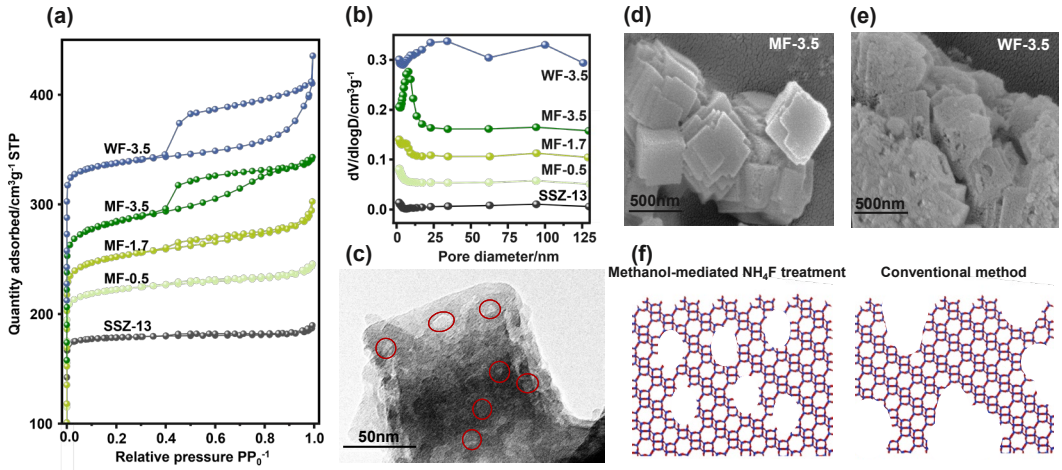

Figure 2. Characterization of hierarchical SSZ-13 zeolite. (a) Ar physisorption isotherms of the pristine and NH_4F-treated SSZ-13 zeolites. (b) The corresponding mesopore size distribution is derived from the adsorption branch of the isotherm based on the BJH model. (c) TEM image of the MF-3.5. SEM image of (d) MF-3.5 and (e) WF-3.5. (f) Illustration of the prepared samples from the proposed method in this work and the conventional NH_4F aqueous solution etching method. The number suffix shows the NH_4F weight concentration. MF: NH_4F-methanol solution treated SSZ-13 zeolite; WF: NH_4F-water solution treated SSZ-13 zeolite.

XRD results show that all the 50°C prepared NH_4F-etched samples maintain good crystallinity (**Table 1**) with a typical CHA topology (**Figure S6**). The similar Si/Al ratios (**Table 1**) of the samples indicate unbiased etching on framework Si and Al atoms, which is typical in fluoride-based etching processes.[32-33] Ar adsorption-desorption isotherms are measured to determine the porosity of pristine SSZ-13 and NH_4F-treated samples. Ar is chosen over N_2 as the adsorbate to evaluate the porosity due to its low reactivity and lack of specific interactions with adsorbent surfaces. The pristine SSZ-13 zeolite displays a typical type-I isotherm for microporous structures (**Figure 2a**). The microporous structure of SSZ-13 is still retained after NH_4F treatments, as seen by the steep increase in Ar adsorption in the low-pressure region ($P/P_0 < 0.1$) for all MF and WF samples.[34] With the increase of NH_4F concentration, the appearance of mesopores, indicated by the hysteresis loop, first appears in the MF-1.7 sample and becomes more pronounced in the MF-3.5 sample. Moreover, the mesopore volume (V_{meso}) and surface area (S_{meso}) gradually increase with the increase of NH_4F

concentration (**Table 1**). Particularly, the mesoporous surface area (107 m^{-2} g^{-1}) and volume (0.12 cm^{-3} g^{-1}) in the MF-3.5 sample are six times higher than those of the pristine SSZ-13 zeolite (18 m^{-2} g^{-1} and 0.02 cm^{-3} g^{-1}, respectively). The nearly linear Ar uptake over P/P_0 = 0.1~0.6 in MF-1.7 and MF-3.5 samples suggests the existence of small mesopores,[35] which is consistent with the 7 nm mesopores observed in the BJH pore size distribution (**Figure 2b**). In stark contrast, the WF-3.5 sample exhibits an obvious mesoporous structure (a conspicuous hysteresis loop) but in the presence of large mesopores or macrospores and a broad pore size distribution ranging from 2 to 125 nm (**Figure 2b**). The large mesopore diameter of the WF sample is also reflected in its low mesopore surface area of only 69 m^2 g^{-1} (**Table 1**). The direct porosity visualization of the MF and WF samples is provided in the TEM images. In contrast to the pristine SSZ-13 sample, which lacks mesopore features, the MF sample shows the larger light contrast areas that are distributed within its crystal, indicating the presence of mesopores (**Figure 2c**). And the WF-3.5 sample displays large mesopores and macrospores within the severely damaged SSZ-13 crystals (**Figure S8b**). In addition to the differences observed in the pore analysis between the MF and WF samples, a remarkable distinction in zeolite morphology is evident in high-resolution scanning electron microscopy (SEM), although the particle size of the SSZ-13 before and after NH_4F treatments (WF-3.5 and MF-3.5) remains similar (**Figure S9)**. The pristine SSZ-13 and MF samples (MF-0.5~3.5) exhibit a smooth surface (**Figure 2d, Figures S8c-e**), which stands in stark contrast to the rough and severely damaged surface of the WF-3.5 sample with many large holes (> 50 nm) (**Figure 2e**). It is worth noting that although adjusting the etching temperature (from 25°C to 80°C) for the NH_4F-water etched SSZ-13, the obtained WF samples are unable to exhibit well-distributed mesopores and their surface remains severely etched (**Figure S10** and **Table S2**).

Table 1. Physicochemical characteristics of the pristine SSZ-13 and the series of NH_4F-treated SSZ-13 zeolites under different conditions.

Sample	[e] *Crystylinity (%)*	[f] *Si/Al framework*	[g] *Si/Al Bulk*	[a] S_{BET} ($m^2 g^{-1}$)	[b] S_{meso} ($m^2 g^{-1}$)	[c] V_{mic} ($cm^3 g^{-1}$)	[d] V_{meso} ($cm^3 g^{-1}$)
SSZ-13	100	9.8	9.4	653	18	0.22	0.02
MF-0.5	103	10.4	9.8	595	54	0.19	0.06
MF-1.7	96	12.8	11.0	541	86	0.16	0.11
MF-3.5	90	14.2	13.9	439	107	0.12	0.12
WF-3.5	83	13.1	12.3	458	69	0.14	0.15

[a] Total surface area. [b] Mesopore surface area, t-plot. [c] Micropore volume, t-plot. [d] Mesopore volume, (V_{total}-V_{mic}). [e] Determined by XRD analysis, see Method in SI. [f] Determined with ^{29}Si MAS SSNMR data in **Figure S7** by the equation: $\sum_{n=0}^{4} I_{Si(OAl)_n} / 0.25 \sum_{n=0}^{4} nSI_{Si(OAl)_n}$, [g] Determined by EDS analysis.

The apparent difference in pore structure and surface morphology between MF and WF samples is illustrated in **Figure 2f**. The well-defined mesopores and smooth surface of the MF samples can be attributed to the in-situ generation of etching species within the zeolite channels. This approach avoids heterogeneous etching caused by diffusion resistance, as opposed to the NH_4F aqueous solution-based method. Therefore, the proposed methanol-mediated NH_4F etching method successfully creates a hierarchical pore structure with both micropores and mesopores within the small-pore SSZ-13 zeolite, which is a significant achievement as it has not been previously realized in small-pore zeolites using post-treatment methods.

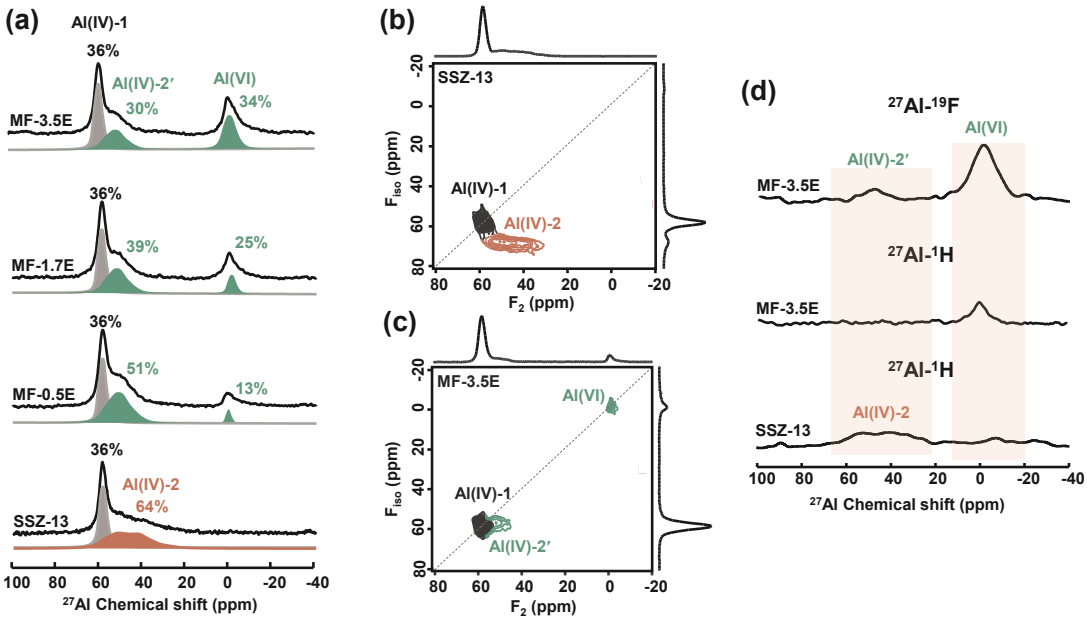

Figure 3. SSNMR characterization of the etching behaviours. (a) Mass normalized quantitative ^{27}Al MAS SSNMR spectra of pristine SSZ-13, MF-0.5E, MF-1.7E, and MF-3.5E samples. ^{27}Al MQ MAS SSNMR spectra of (b) pristine SSZ-13 and (c) MF-3.5E samples. (d) ^{27}Al(^{1}H)/^{27}Al(^{19}F) CP MAS SSNMR spectra of pristine SSZ-13 and MF-3.5E samples. A short contact time of 50 μs was employed to ensure that the prominent peaks represent directly bonded Al-F species.[36]

The distinct and precisely defined pore structure achieved via the methanol-mediated NH_4F etching method prompt us to study the etching mechanism and mesopore generation. To gain insight into these aspects, solid-state nuclear magnetic resonance (SSNMR) spectroscopy is employed to explore the framework coordination changes of Si and Al atoms, the etchant F atoms, and the H atoms within the SSZ-13 channels. To preserve the etched species, methanol in the samples is removed by evaporation after the NH_4F-methanol etching process, and the resulting samples are labelled as MF-0.5E, MF-1.7E, and MF-3.5E, respectively. **Figure 3a** depicts the one-dimensional (1D) ^{27}Al Magic Angle Spinning (MAS) SSNMR spectra of the pristine SSZ-13 and the MF-0.5E, MF-1.7E, and MF-3.5E samples. For the pristine SSZ-13, the sharp signal at 60 ppm zeolites is attributed to tetrahedral framework Al sites, designated as Al(IV)-1 (**Figure 3a**). In addition, a broad peak with a chemical shift of 20-60 ppm is present, which can be better resolved in the 2D ^{27}Al multiple-quantum (MQ) MAS SSNMR spectrum (**Figure 3b**). This peak is attributed to the partially coordinated framework Al atoms with OH groups ($(SiO)_{4-n}Al(OH)_n$, n = 1~3), commonly known as Al(IV)-2, which usually results from the synthesis process and post-treatment.[37-40] Further evidence for the structure of Al(IV)-2 in the pristine SSZ-13 can be seen in the ^{1}H double-quantum (DQ) MAS SSNMR experiment (**Figure S11**), where it is identified as $(SiO)_3Al(OH)$.

After the NH_4F-methanol treatment, a shift in the Al(IV)-2 signal is observed, which moves to the range of 40-60 ppm and is labelled as Al(IV)-2', while the Al(IV)-1 peak remains unchanged (**Figure 3a**). Al(IV)-2' signal can be clearly distinguished from Al(IV)-2 in the 2D ^{27}Al MQ MAS SSNMR spectrum **(Figure 3c and Figure S12)**. Simultaneously, a peak at 0 ppm corresponding to the extra-framework six-coordinated aluminium species emerges, labelled as Al(VI).[40] To evaluate the different coordination environments around Al atoms, isotropic chemical shifts (δ_{iso}) and second-order quadrupolar interaction constants (C_q) are extracted from MQ MAS SSNMR spectra. As shown in **Table S3**, the Al(IV)-2' of the MF-0.5E, MF-1.7E, and MF-3.5E samples exhibit close

chemical shift values but a smaller C_q value than the Al(IV)-2 in pristine SSZ-13. This suggests that the coordination environment of Al(IV)-2' is less distorted than that of Al(IV)-2 species, indicating a change in coordination during the etching process.

To study the proximity information of the Al(IV)-2' species, $^{27}Al(^{1}H)$ and $^{27}Al(^{19}F)$ cross-polarization (CP) MAS SSNMR experiments are performed. The $^{27}Al(^{1}H)$ CP MAS SSNMR spectrum shows the Al(IV)-2 signal (20-60 ppm) due to the close spatial proximity between H and Al of $(SiO)_3Al(OH)$ in the pristine SSZ-13 (**Figure 3d**). After NH_4F-methanol treatment (the MF-3.5E sample), the Al(IV)-2 signal in the $^{27}Al(^{1}H)$ CP MAS SSNMR spectrum disappears, and concurrently, the signal at 40-60 ppm appears in the $^{27}Al(^{19}F)$ CP MAS SSNMR spectrum. Similar results are observed in the $^{27}Al(^{1}H)$ and $^{27}Al(^{19}F)$ CP MAS SSNMR experiments of MF-0.5E and MF-1.7E samples (see **Figure S13**). The 40-60 ppm peak observed in the $^{27}Al(^{19}F)$ CP MAS SSNMR spectrum indicates a short distance between Al and F atoms in Al(IV)-2' sites. In other words, NH_4F-methanol treatment converts $(SiO)_3Al(OH)$ (i.e., Al(IV)-2) in SSZ-13 to $(SiO)_3Al$-F (i.e., Al(IV)-2'). The quantified 1D ^{27}Al MAS NMR spectra in **Figure 3a** reveal that as NH_4F concentration increases, the ratios of Al(IV)-2' decrease from 51% in MF-0.5E to 39% in MF-1.7E and 30% in MF-3.5E, while the ratios of Al(VI) increase from 13% in MF-0.5E to 25% in MF-1.7E and 34% in MF-3.5E. It is important to note that the ratio of the Al(IV)-1 peak remains unchanged at 36%. Therefore, the conversion of tetrahedral Al(IV)-2' species to octahedral extra-framework Al(VI) sites must occur, presumably by further breaking the framework Al-O bonds of Al(IV)-2' during the etching process under high NH_4F concentration condition.

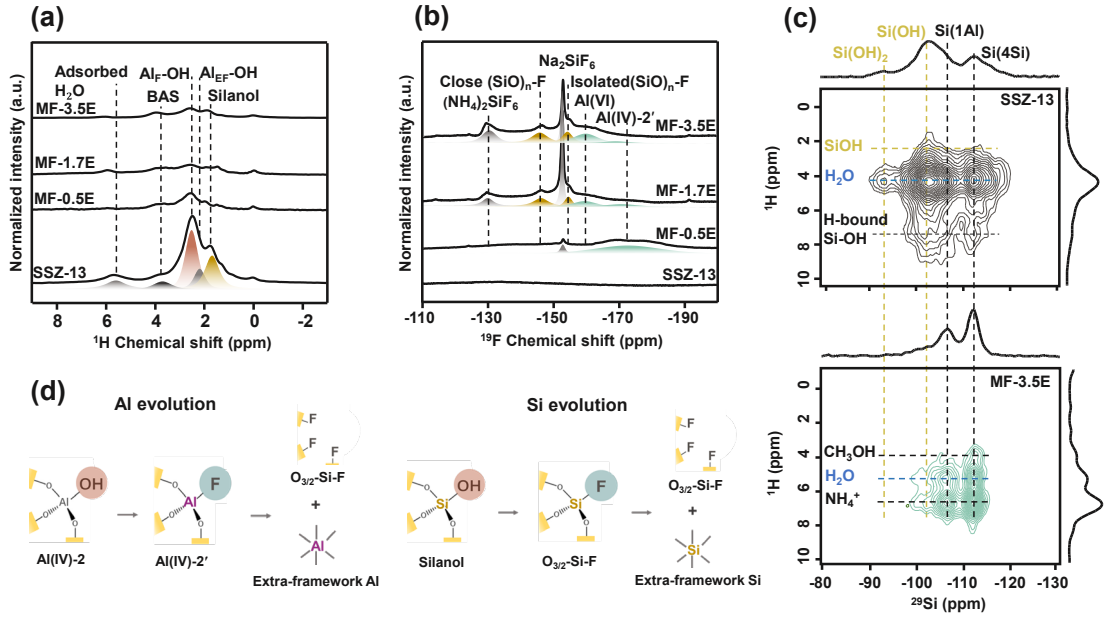

Figure 4. SSNMR characterization of the etching behaviours. (a) ^{1}H and (b) ^{19}F MAS SSNMR spectra of the pristine SSZ-13 and MF-0.5E~3.5E samples. ^{19}F MAS SSNMR spectra were collected with a rotor-synchronized spin-echo sequence with an echo time of 55.6 μs (spinning frequency= 18 kHz). (c) $^{29}Si(^{1}H)$ HETCOR MAS SSNMR spectra of the pristine SSZ-13 and the MF-3.5E sample with a contact time of 4 ms, the corresponding spectra with contact time at 0.4 ms are displayed in **Figure S19**. The assignments for the signals in the F1 and F2 projections can be found in **Figure S18**. (d) Illustration of Al and Si evolution during the mesopore formation.

The above results have demonstrated that the etching process starts from the partially coordinated framework Al-OH sites (Al(IV)-2). To gain further insights from the environment of the hydroxyl species and its associated changes after the NH_4F-methanol treatment, ^{1}H MAS SSNMR spectra of

the dehydrated pristine SSZ-13 and the MF-0.5E~3.5E samples are collected. The purpose of dehydration is to allow for the clear identification of hydroxyl species. From **Figure 4a**, the dehydrated SSZ-13 exhibits signals with chemical shifts at 1.7, 2.4, 2.7, 3.8, and 5.5 ppm, corresponding to the framework silanols, extra-framework Al-OH (Al_{EF}-OH), framework Al-OH (Al_F-OH) in Al(IV)-2, Brønsted acid sites, and strongly adsorbed water molecules, respectively.[40-41] After the NH_4F-methanol treatment, the peak intensity of the Al_F-OH decreases significantly for all the MF samples due to the conversion of Al(IV)-2 to Al(IV)-2', as discussed before (**Figure 3**). Similarly, the silanol peak also shows a noticeable decrease, suggesting silanols are also converted in the etching process.

^{19}F MAS SSNMR is also conducted, as shown in **Figure 4b**, to resolve the observed local structure changes from the perspective of F atoms. The result shows that no peaks are observed in the pristine SSZ-13, indicating the absence of F contamination in our pristine zeolite. After treatment with low NH_4F concentration, for the MF-0.5E sample, two peaks at -180 and -153 ppm are identified. The former is attributed to Al(IV)-2', as confirmed by $^{27}Al(^{19}F)$ HETCOR SSNMR spectrum (**Figure S14**), while the latter is attributed to Na_2SiF_6, as confirmed by the standard reference (**Figure S15**), suggesting some Si atoms are eliminated from frameworks by the fluoride treatment and finally form Na_2SiF_6 with Na in the zeolite. At higher NH_4F concentrations, the extra-framework octahedral Al(VI) can be observed, as confirmed in the $^{27}Al(^{19}F)$ HETCOR spectrum (**Figure S14**), in line with our previous ^{27}Al SSNMR results. In addition, the peak of Na_2SiF_6 species significantly increases in the MF-1.7E and MF-3.5E samples (as shown in **Figure 4b**). A signal at -129 ppm, assigned to $(NH_4)_2SiF_6$ as confirmed by the standard reference (**Figure S15**), can also be seen at higher NH_4F concentrations, which is also identified in the XRD pattern (**Figure S16**). Furthermore, peaks at -155 and -146 ppm observed in the MF-1.7E and MF-3.5E samples are attributed to tetrahedral framework $O_{3/2}$-Si-F (isolated or two in proximity, respectively).[42] The presence of $O_{3/2}$-Si-F in the NH_4F-treated samples confirms the previously observed conversion of the framework silanol structure (in ^1H NMR spectra, **Figure 4a**) to Si-F species, and it also implies that there may be newly formed defects terminated by F atoms due to continuous framework Si and Al eliminations.

Figure 4d summarizes the above observations: Fluoridation occurs at the Al-OH and Si-OH site by replacing -OH with -F, and the extraction of framework Si and Al atoms occurs during the NH_4F-methanol treatment, forming the extra-framework Al, Na_2SiF_6 and $(NH_4)_2SiF_6$, creating more exposed framework Si and Al for further fluoridation. It is worth noting that the fluoridation of Si-OH and Al-OH groups can only be achieved by the etching species produced via NH_4F hydrolysis, as non-nucleophilic F^- anions alone are not effective in reacting with hydroxyl groups.[27] This is supported by comparing the etching of pristine SSZ-13 and dehydrated SSZ-13 using an NH_4F methanol solution. Notably, unlike the hydrated SSZ-13 (**Figure S17**), the treatment of dehydrated SSZ-13 does not lead to a reduction in the Si-OH or Al-OH peaks nor the generation of Si-F or Al-F species (Na_2SiF_6 and Al(IV)-2' sites). This finding indicates that the hydrolysis of F^-/NH_4F (leading to the release of etching species such as HF and HF_2^-),[15,27] initiated by the water in the zeolite, is a crucial step for fluoridation and the subsequent removal of framework Al and Si.

Considering the important role of H_2O molecules in the formation of etching species, $^{29}Si(^1H)$ HETCOR MAS SSNMR experiments are conducted to map the proximity of H_2O in the zeolitic channels with the framework silanols. Note that the $^{27}Al(^1H)$ HETCOR MAS SSNMR experiments have also been attempted to study the H_2O proximity with Al(IV)-2 sites, but were unsuccessful due to its large quadrupolar coupling constant (C_q) leading to more rapid relaxation of the ^{27}Al spin and

a reduction in the dipolar coupling efficiency.[43] For the pristine SSZ-13, as shown in **Figure 4c**, two correlation peaks are observed between H_2O and defect silanol species (Si-$(OH)_2$ and Si-OH)(**Figure S18**), and the intensity of both peaks remains virtually unchanged even after shortening the contact time from 4 ms to 0.4 ms (**Figure S19**). This indicates close spatial proximity between H_2O molecules and defect silanols. In contrast, although the correlation peak between H_2O and Si(4Si) units occurs, the peak intensity significantly decreases with shortening contact time (**Figure S19)**, suggesting a long distance between them. After fluoride treatment, the correlation peaks corresponding to defect silanol species and H_2O molecules disappear due to the reactions of silanol defects with fluoride etching species, as discussed before. Consequently, from $^{29}Si(^{1}H)$ HETCOR MAS SSNMR experiments, we can confirm H_2O is in proximity to the silanol sites, and it is reasonable to infer that the H_2O is also in proximity to the framework-associated Al-OH defects as hydroxyl species are commonly associated with zeolite hydrophilicity.[44]

From the above results, we can conclude the etching mechanism of this methanol-mediated NH_4F post-treatment strategy, as illustrated in **Figure 5.** The term "Trojan Horse-like Introduction and Activation" is used to evoke the metaphorical concept of hidden reactivity of NH_4F and in-situ release of active etching species in the process: (1) Inert etching agent, F^-/NH_4F, is first introduced into the internal channels of the zeolite in methanol solution; (2) The etching process is initiated by the in-situ release of fluoride etching species via F^- hydrolysis at the location of water-enriched defect sites, including Al-OH of Al(IV)-2 and silanols, in the channels of the zeolite; (3) These active species interact with the framework Al-OH and Si-OH to form framework Al-F and Si-F species; (4) The additional framework Al-O and Si-O bonds in the defects are broken continuously with further etching; (5) The framework Si and Al atoms are extracted as extra-framework octahedral species; (6) The extra-framework species are washed out by water **(Figure S20)**, leaving the mesopore and the intrinsic micropore in the zeolite.

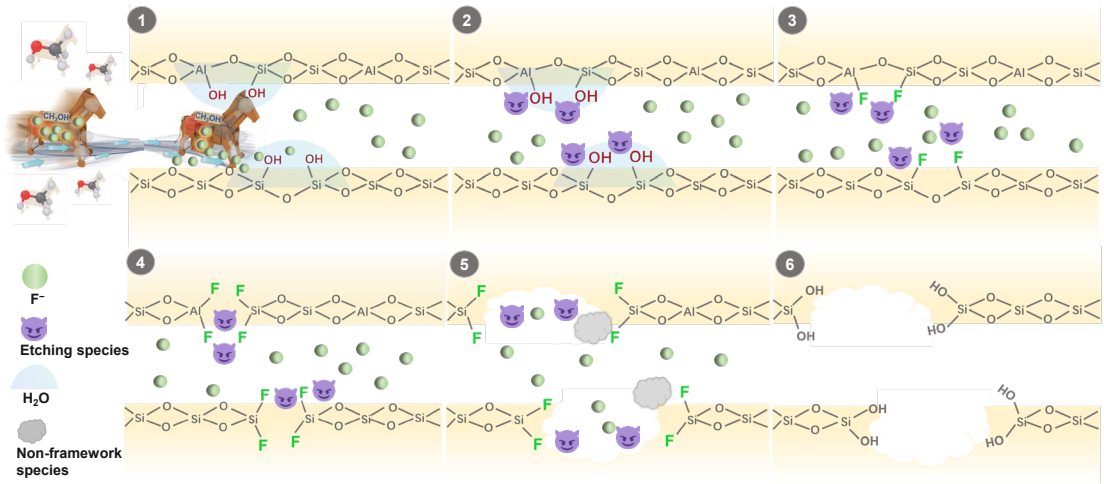

Figure 5. Proposed mechanism for the formation of hierarchically structured SSZ-13 zeolite through the "Trojan Horse-like" NH_4F introduction and hydrolysis activation strategy.

Conclusion

This research introduces a novel strategy for hydrolysis-triggered in-situ pore engineering in zeolites, drawing inspiration from the Trojan Horse concept. By utilizing the initially inert NH_4F in methanol, we successfully transport the etching species with hidden reactivity into the small pore SSZ-13 zeolite. Through in-situ hydrolysis of the introduced F^- anions within the zeolite channels, active etching species are generated, thereby circumventing the issues of heterogeneous etching and

morphology disruption commonly observed in small pore zeolites during the diffusion-resistant aqueous NH_4F etching process. Our method successfully generates well-distributed mesopores with a narrow pore size distribution (approximately 7 nm) throughout SSZ-13. Atomic-scale analysis using solid-state NMR spectroscopy has mapped the Si and Al evolution during the etching process, identifying two types of defects, Al(IV)-2 and silanols, as the starting points for etching. Both sites can be initially converted to framework Al-F and Si-F species, which are then extracted as extra-framework octahedral Si and Al species as the etching process progresses, leading to mesopore formation. The proposed method offers several advantages for tailoring porosity in zeolites and has the potential to advance the field of zeolite post-treatment technology by providing a uniform and controllable hierarchical pore engineering approach.

Conflicts of interest

There are no conflicts of interest to declare.

Author contributions

Youdong Xing: conceptualization, validation, investigation, methodology, data curation, visualization, writing & editing. Guangchao Li: guide, methodology, data curation, discussion, writing & editing. Zezhou Lin & Haitao Huang: visualization, discussion. Zhihang Xu & Ye Zhu: data curation, visualization, discussion. Shik Chi Edman Tsang: guide, discussion. Molly Meng-Jung Li: supervision, funding acquisition, project administration, guide, discussion, writing & editing.

Acknowledgments

The authors wish to thank the financial support from The Department of Science and Technology of Guangdong Province (2021A1515010021), RGC Hong Kong (PolyU P0033541, PolyU P0036828), and Shenzhen Science and Technology Innovation Commission (JCYJ20210324140811032).

References

1. Wu, S. M.; Yang, X. Y.; Janiak, C., Confinement Effects in Zeolite-Confined Noble Metals. *Angewandte Chemie International Edition* **2019**, *131*, 12468-12482.
2. Dubbeldam, D.; Calero, S.; Maesen, T. L.; Smit, B., Incommensurate Diffusion in Confined Systems. *Physical review letters* **2003**, *90*, 245901.
3. Scott, S. L., Bioinspired Methane Oxidation in a Zeolite. *Science* **2021**, *373*, 277-278.
4. Dusselier, M.; Van Wouwe, P.; Dewaele, A.; Jacobs, P. A.; Sels, B. F., Shape-Selective Zeolite Catalysis for Bioplastics Production. *Science* **2015**, *349*, 78-80.
5. Bai, R.; Song, Y.; Li, Y.; Yu, J., Creating Hierarchical Pores in Zeolite Catalysts. *Trends in Chemistry* **2019**, *1*, 601-611.
6. Lopez-Orozco, S.; Inayat, A.; Schwab, A.; Selvam, T.; Schwieger, W., Zeolitic Materials with Hierarchical Porous Structures. *Advanced Materials* **2011**, *23*, 2602-2615.
7. Lakiss, L.; Kouvatas, C.; Gilson, J. P.; Aleksandrov, H. A.; Vayssilov, G. N.; Nesterenko, N.; Mintova, S.; Valtchev, V., Unlocking the Potential of Hidden Sites in Faujasite: New Insights in a Proton Transfer Mechanism. *Angewandte Chemie International Edition* **2021**, *133*, 26906-26913.
8. Zhu, X.; Hofmann, J. P.; Mezari, B.; Kosinov, N.; Wu, L.; Qian, Q.; Weckhuysen, B. M.; Asahina, S.; Ruiz-Martínez, J.; Hensen, E. J., Trimodal Porous Hierarchical SSZ-13 Zeolite with Improved Catalytic Performance in the Methanol-to-Olefins Reaction. *ACS Catalysis* **2016**, *6*, 2163-2177.
9. Shamzhy, M.; Opanasenko, M.; Concepción, P.; Martínez, A., New Trends in Tailoring Active Sites in Zeolite-Based Catalysts. *Chemical Society Reviews* **2019**, *48*, 1095-1149.
10. Wei, Y.; Parmentier, T. E.; de Jong, K. P.; Zečević, J., Tailoring and Visualizing the Pore Architecture of Hierarchical Zeolites. *Chemical Society Reviews* **2015**, *44*, 7234-7261.
11. Zukal, A.; Patzelova, V.; Lohse, U., Secondary Porous Structure of Dealuminated Y Zeolites. *Zeolites* **1986**, *6*, 133-136.
12. Sommer, L.; Mores, D.; Svelle, S.; Stöcker, M.; Weckhuysen, B. M.; Olsbye, U., Mesopore Formation in Zeolite H-SSZ-13 by Desilication with NaOH. *Microporous and Mesoporous Materials* **2010**, *132*, 384-394.
13. Janssen, A. H.; Koster, A. J.; de Jong, K. P., Three-Dimensional Transmission Electron Microscopic Observations of Mesopores in Dealuminated Zeolite Y. *Angewandte Chemie International Edition* **2001**, *40*, 1102-1104.
14. Yang, S.; Yu, C.; Yu, L.; Miao, S.; Zou, M.; Jin, C.; Zhang, D.; Xu, L.; Huang, S., Bridging Dealumination and Desilication for the Synthesis of Hierarchical MFI Zeolites. *Angewandte Chemie International Edition* **2017**, *56*, 12553-12556.
15. Qin, Z.; Lakiss, L.; Gilson, J. P.; Thomas, K.; Goupil, J. M.; Fernandez, C.; Valtchev, V., Chemical Equilibrium Controlled Etching of MFI-Type Zeolite and Its Influence on Zeolite Structure, Acidity, and Catalytic Activity. *Chemistry of Materials* **2013**, *25*, 2759-2766.
16. Knotter, D. M., The Chemistry of Wet Etching. *Handbook of Cleaning in Semiconductor Manufacturing: Fundamental and Applications* **2010**, 95-141.
17. Hong, Z.; Li, L.; Miao, L.; Zhao, G.; Zhu, Z., Opening Sodalite Cages of X Zeolite for Boosting Toluene Side-Chain Alkylation Performance. *Catalysis Science & Technology* **2023**, *13*, 1991-1995.
18. Qin, Z.; Cychosz, K. A.; Melinte, G.; El Siblani, H.; Gilson, J. P.; Thommes, M.; Fernandez, C.; Mintova, S.; Ersen, O.; Valtchev, V., Opening the Cages of Faujasite-Type Zeolite. *Journal of the American Chemical Society* **2017**, *139*, 17273-17276.
19. Qin, Z.; Hafiz, L.; Shen, Y.; Daele, S. V.; Boullay, P.; Ruaux, V.; Mintova, S.; Gilson, J.-P.; Valtchev,

V., Defect-Engineered Zeolite Porosity and Accessibility. *Journal of Materials Chemistry A* **2020**, *8*, 3621-3631.

20. Chen, X.; Xi, D.; Sun, Q.; Wang, N.; Dai, Z.; Fan, D.; Valtchev, V.; Yu, J., A Top-Down Approach to Hierarchical SAPO-34 Zeolites with Improved Selectivity of Olefin. *Microporous and Mesoporous Materials* **2016**, *234*, 401-408.

21. Qin, Z.; Pinard, L.; Benghalem, M. A.; Daou, T. J.; Melinte, G.; Ersen, O.; Asahina, S.; Gilson, J.-P.; Valtchev, V., Preparation of Single-Crystal "House-of-Cards"-Like ZSM-5 and Their Performance in Ethanol-to-Hydrocarbon Conversion. *Chemistry of Materials* **2019**, *31*, 4639-4648.

22. Chen, X.; Todorova, T.; Vimont, A.; Ruaux, V.; Qin, Z.; Gilson, J.-P.; Valtchev, V., In Situ and Post-Synthesis Control of Physicochemical Properties of FER-Type Crystals. *Microporous and mesoporous materials* **2014**, *200*, 334-342.

23. Qin, Z.; You, Z.; Bozhilov, K. N.; Kolev, S. K.; Yang, W.; Shen, Y.; Jin, X.; Gilson, J. P.; Mintova, S.; Vayssilov, G. N., Dissolution Behavior and Varied Mesoporosity of Zeolites by NH_4F Etching. *Chemistry–A European Journal* **2022**, *28*, e202104339.

24. Qin, Z.; Gilson, J.-P.; Valtchev, V., Mesoporous Zeolites by Fluoride Etching. *Current Opinion in Chemical Engineering* **2015**, *8*, 1-6.

25. Yoshioka, T.; Iyoki, K.; Hotta, Y.; Kamimura, Y.; Yamada, H.; Han, Q.; Kato, T.; Fisher, C. A.; Liu, Z.; Ohnishi, R., Dealumination of Small-Pore Zeolites through Pore-Opening Migration Process with the Aid of Pore-Filler Stabilization. *Science Advances* **2022**, *8*, eabo3093.

26. Babić, V.; Koneti, S.; Moldovan, S.; Nesterenko, N.; Gilson, J.-P.; Valtchev, V., Preparation of Hierarchical SSZ-13 by NH_4F Etching. *Microporous and Mesoporous Materials* **2021**, *314*, 110863.

27. Knotter, D. M., Etching Mechanism of Vitreous Silicon Dioxide in HF-Based Solutions. *Journal of the American Chemical Society* **2000**, *122*, 4345-4351.

28. Tressaud, A., Fluorine, a Key Element for the 21st Century. *Fluorine; Tressaud, A., Ed.; Elsevier: Amsterdam, The Netherlands* **2019**, *5*, 77-150.

29. Spierings, G., Wet Chemical Etching of Silicate Glasses in Hydrofluoric Acid Based Solutions. *Journal of Materials Science* **1993**, *28*, 6261-6273.

30. Corbett, C. A.; Martínez, T. J.; Lisy, J. M., Solvation of the Fluoride Anion by Methanol. *The Journal of Physical Chemistry A* **2002**, *106*, 10015-10021.

31. Gerken, M.; Boatz, J.; Kornath, A.; Haiges, R.; Schneider, S.; Schroer, T.; Christe, K., The ^{19}F NMR Shifts Are Not a Measure for the Nakedness of the Fluoride Anion. *Journal of fluorine chemistry* **2002**, *116*, 49-58.

32. Qin, Z.; Melinte, G.; Gilson, J. P.; Jaber, M.; Bozhilov, K.; Boullay, P.; Mintova, S.; Ersen, O.; Valtchev, V., The Mosaic Structure of Zeolite Crystals. *Angewandte Chemie International Edition* **2016**, *128*, 15273-15276.

33. Bozhilov, K. N.; Le, T. T.; Qin, Z.; Terlier, T.; Palčić, A.; Rimer, J. D.; Valtchev, V., Time-Resolved Dissolution Elucidates the Mechanism of Zeolite MFI Crystallization. *Science Advances* **2021**, *7*, eabg0454.

34. Wu, L.; Degirmenci, V.; Magusin, P. C.; Lousberg, N. J.; Hensen, E. J., Mesoporous SSZ-13 Zeolite Prepared by a Dual-Template Method with Improved Performance in the Methanol-to-Olefins Reaction. *Journal of Catalysis* **2013**, *298*, 27-40.

35. Wang, H.; Pinnavaia, T. J., MFI Zeolite with Small and Uniform Intracrystal Mesopores. *Angewandte Chemie International Edition* **2006**, *118*, 7765-7768.

36. Kao, H.-M.; Liao, Y.-C., Direct Solid-State NMR Observation of Tetrahedral Aluminum Fluorides

in Zeolite HY Fluorinated by Ammonium Fluoride. *The Journal of Physical Chemistry C* **2007**, *111*, 4495-4498.

37. Chen, K.; Horstmeier, S.; Nguyen, V. T.; Wang, B.; Crossley, S. P.; Pham, T.; Gan, Z.; Hung, I.; White, J. L., Structure and Catalytic Characterization of a Second Framework Al (IV) Site in Zeolite Catalysts Revealed by NMR at 35.2 T. *Journal of the American Chemical Society* **2020**, *142*, 7514-7523.

38. Chen, K.; Zornes, A.; Nguyen, V.; Wang, B.; Gan, Z.; Crossley, S. P.; White, J. L., ^{17}O Labeling Reveals Paired Active Sites in Zeolite Catalysts. *Journal of the American Chemical Society* **2022**, *144*, 16916-16929.

39. Chen, K.; Gan, Z.; Horstmeier, S.; White, J. L., Distribution of Aluminum Species in Zeolite Catalysts: ^{27}Al NMR of Framework, Partially-Coordinated Framework, and Non-Framework Moieties. *Journal of the American Chemical Society* **2021**, *143*, 6669-6680.

40. Fan, B.; Zhu, D.; Wang, L.; Xu, S.; Wei, Y.; Liu, Z., Dynamic Evolution of Al Species in the Hydrothermal Dealumination Process of CHA Zeolites. *Inorganic Chemistry Frontiers* **2022**, *9*, 3609-3618.

41. Wang, M.; Jaegers, N. R.; Lee, M.-S.; Wan, C.; Hu, J. Z.; Shi, H.; Mei, D.; Burton, S. D.; Camaioni, D. M.; Gutiérrez, O. Y., Genesis and Stability of Hydronium Ions in Zeolite Channels. *Journal of the American Chemical Society* **2019**, *141*, 3444-3455.

42. Hartmeyer, G.; Marichal, C.; Lebeau, B.; Caullet, P.; Hernandez, J., Fluorination of Silica Nanoparticles by Aqueous NH_4F Solutions. *The Journal of Physical Chemistry C* **2007**, *111*, 6634-6644.

43. Chen, K., A Practical Review of Nmr Lineshapes for Spin-1/2 and Quadrupolar Nuclei in Disordered Materials. *International Journal of Molecular Sciences* **2020**, *21*, 5666.

44. Iyoki, K.; Kikumasa, K.; Onishi, T.; Yonezawa, Y.; Chokkalingam, A.; Yanaba, Y.; Matsumoto, T.; Osuga, R.; Elangovan, S. P.; Kondo, J. N., Extremely Stable Zeolites Developed Via Designed Liquid-Mediated Treatment. *Journal of the American Chemical Society* **2020**, *142*, 3931-3938.